Stacking Characteristics of Close Packed Materials

Christian H. Loach and Graeme J. Ackland
School of Physics and Astronomy, SUPA, The University of Edinburgh, Edinburgh EH9 3JZ, United Kingdom
(Received 19 June 2017; revised manuscript received 2 August 2017; published 14 November 2017)

It is shown that the enthalpy of any close packed structure for a given element can be characterized as a linear expansion in a set of continuous variables α_n, which describe the stacking configuration. This enables us to represent the infinite, discrete set of stacking sequences within a finite, continuous space of the expansion parameters H_n. These H_n determine the stable structure and vary continuously in the thermodynamic space of pressure, temperature, or composition. The continuity of both spaces means that only transformations between stable structures adjacent in the H_n space are possible, giving the model predictive as well as descriptive ability. We calculate the H_n using density functional theory (DFT) and interatomic potentials for a range of materials. Some striking results are found: e.g., the Lennard-Jones potential model has 11 possible stable structures and over 50 phase transitions as a function of cutoff range. The very different phase diagrams of Sc, Tl, Y, and the lanthanides are understood within a single theory. We find that the widely reported 9R-fcc transition is not allowed in equilibrium thermodynamics, and in cases where it has been reported in experiments (Li, Na), we show that DFT theory is also unable to predict it.

DOI: 10.1103/PhysRevLett.119.205701

In 1611, Kepler suggested that stackings of triangular layers was the most efficient way to pack hard spheres [1]. This conjecture was only recently proved [2].

Many elements crystallize in close packed crystal structures, but the concept of "close packed" is not part of crystallographic categorization. This is because there are an infinite number of Keplerian stacking arrangements with equal packing density, spanning a wide range of space group symmetries. Most observed structures have short repeat sequences such as face-centered cubic (fcc) or hexagonal close packed (hcp), but there is no general theory to explain why these should have the lowest energy.

Predicting the stable crystal structure for a material is a longstanding challenge in condensed matter physics. One underlying reason is that crystal structures are defined by discrete symmetry groups and integer numbers of atoms per unit cell. Aside from the atomic positions themselves, there are no continuous variables which cover the entire space of possibilities; thus, we are searching for a minimum in a discontinuous space.

Among close packed structures, only fcc has close packing enforced by symmetry. For all other stackings, there is an "ideal" ratio between interlayer spacing and interatomic separation ($c/a = \sqrt{2/3}$) which gives close packing. Generally, materials adopting structures within a few percent of ideal are regarded as close packed.

Stacking sequences are typically defined as a series of layers labeled A, B, and C with atoms positioned at $0\mathbf{a} + 0\mathbf{b}$; $\frac{1}{3}\mathbf{a} + \frac{1}{3}\mathbf{b}$; and $\frac{2}{3}\mathbf{a} + \frac{2}{3}\mathbf{b}$, respectively, where $\mathbf{a}$ and $\mathbf{b}$ are the in-plane lattice vectors. This ABC notation is not unique: a more compact notation [3] uses h for layers with identical neighbors (ABA), f for those with different (ABC). For examples see Table I.

The most widely used model for atomistic modeling is the Lennard-Jones potential, which describes the van der Waals bonding of inert gases. It has hcp as the most stable structure at low temperature, transforming to fcc at high temperature [4].

More sophisticated modeling of electronic structure using density functional theory (DFT) can be applied across the periodic table, and gives quantitative agreement with experiment [5] although it is impossible to check all possible stacking sequences.

In this Letter we show that the energies of the infinity of stacking sequences can be represented by a convergent series, and that phase boundaries between some pairs of crystal structures cannot occur. We demonstrate the extraordinary sensitivity of the Lennard-Jones phase diagram to the potential cutoff. We show that deviations from ideal c/a ratios are correlated with stability. We also investigate the

TABLE I. Representation of various structures in terms of basal stacking in the different notations. Note that ABC and ACB represent the same structure, fcc, and that structures are not uniquely defined by α_2, α_3.

Name	ABC	hf	Minimal	α_2	α_3
hcp	AB	hh	h	1	0
fcc	ABC	fff	f	0	1
fcc	ACB	fff	f	0	1
dhcp	ABCB	hfhf	hf	1/2	0
	ABCAB	hffh	hffh	2/5	2/5
9R	ABACACBCB	hhfhhfhhf	hhf	2/3	0

role of pressure and uncover some deep-seated inadequacies in interatomic potentials.

To define the stacking sequence with periodicity M, we introduce a set of parameters α_n

$$\alpha_n = \sum_{i=1}^{M} \frac{\delta_{i,i+n}}{M}, \quad (1)$$

where $\delta_{i,i+n}$ is 1 when the i and $i+n$ layers have the same ABC symbol, and 0 otherwise. Physically, α_n can be thought of as the fraction of the atomic positions $\mathbf{R_i}$ for which there is another atom at $\mathbf{R}_i + n\mathbf{c}$, where c is the interlayer separation. As $M \to \infty$, or for an arbitrary density of stacking faults, the αs become continuous variables.

The set of α's up to α_M univocally describes any possible stacking with an M fold or fewer periodicity. All translationally, rotationally or reflectionally equivalent stackings have the same unique set of α_n, unlike the ABC and hf notations which have considerable redundancy. Trivially, $\alpha_0 = 1$ and $\alpha_1 = 0$ for all close packed structures. Only certain ranges of α_ns correspond to physically realizable structures (see Fig. 1).

We used the CASTEP DFT package [6] to examine a wide selection of elements known to adopt close packed structures. Well-converged energies for various stackings and pressures were determined using the Perdew-Burke-Ernzerhof exchange-correlation functional [7]. In addition to the DFT calculations, we calculate energies of the same structure set using a number of interatomic potentials, both pairwise and many-body, which were fitted to represent the same materials. Our structure set consists of all 43 possible stacking sequences for up to 10 atomic layer repeats in the ABC notation (cf. Table I) excluding redundant strings (i.e., those with identical α_n). Calculations are performed starting from hexagonal style unit cells with cell angles 90°, 90°, 60°; internal coordinates and lattice parameters were fully relaxed and double checked to ensure that each structure remained in its initial metastable state, with each atom in the structure retaining 12-fold coordination and undergoing only small distortion from close packing.

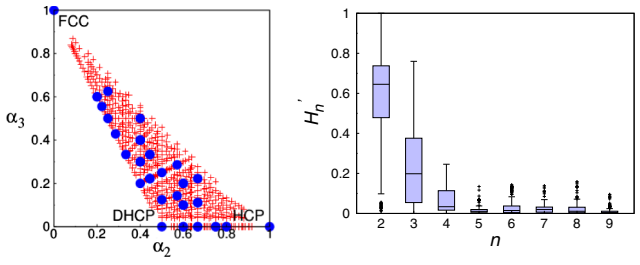

FIG. 1. (left) Physically realizable stackings projected onto the α_2-α_3 plane. Configurations for up to 25 atomic-layer repeats are shown in red. Blue points indicate the 43 structures used in our calculations. (right) Tukay box plots of normalized enthalpy H'_n vs n showing the rapid convergence of Eq. (2). Data are taken from DFT calculations across all elements and pressures. The structure-independent H_0 are omitted. The normalization is defined by $H'_n = (|H_n| / \sum_{i=2}^{9} |H_i|)$.

Using these results, each material is characterized by parameters H_n obtained by a least squares fit to the 43 calculated enthalpies assuming a linear dependence on α_n,

$$H = H_0 + \sum_{n=2} H_n \alpha_n. \quad (2)$$

Every material is, therefore, represented as a point in an N-dimensional H_n space, and every point in the H_n space has an associated most-stable stacking structure calculated by minimizing Eq. (2) with respect to α_n. For example, consider the summation in Eq. (2) up to only $n = 3$, the enthalpy varies linearly with α_2 and α_3, and it follows that the most stable structure must be located at a corner of the triangle of physically possible states shown in Fig. 1(a), allowing only fcc, hcp, or dhcp. More complex structures may be stable if considering H_4 and higher terms.

The H_2 and H_3 values for a range of materials and pressures are shown in Fig. 2(a). The residuals in the fit to DFT data are of order tenths of meV per atom, about 1% of the enthalpy differences between structures. For Eq. (2) to be useful it must be rapidly convergent, and in Fig. 1(b) we show that the terms do indeed decay rapidly with n. Typically, the H_2 and H_3 contributions are dominant.

The key to the usefulness of this result is that we have transformed the discrete representation (ABC or hf) of the crystal structure to a continuous representation (α_n). The phase stability regions in the associated H_n space are material independent, and any stacking sequence will have some region of stability if N is large enough [9]. Geometrically, these regions are hyperpyramids which meet at the origin. We thus predict that transformations between phases whose stability regions are nonadjacent in H_n space (Fig. 3), such as fcc and 9R, are not thermodynamically possible *in any system* if the H_n representation converges.

If we change thermodynamic parameters continuously, the H_i change continuously, tracing a path through the H_n space. This can be evaluated using, e.g., DFT calculations at different pressures. This enables us to anticipate phase transitions arising from continuously changing thermodynamic variables such as temperature, pressure, or composition whenever this path crosses from the stability region of one phase to another. Figure 2(a) shows such trajectories projected into (H_2, H_3) subspace for pressures up to 20 GPa. The clustering of elements' H_2 and H_3 values and the similarities of their pressure dependence corresponds to periodic table groupings, indicating an electronic origin of the observed properties.

Many further inferences can be drawn from the H_n space; for example, Group 11 metals lie close to the origin, and low values of H_n suggest changes in α are not energetically costly. As a consequence, stacking faults (incremental change in α_n) have low energy, meaning that dislocations

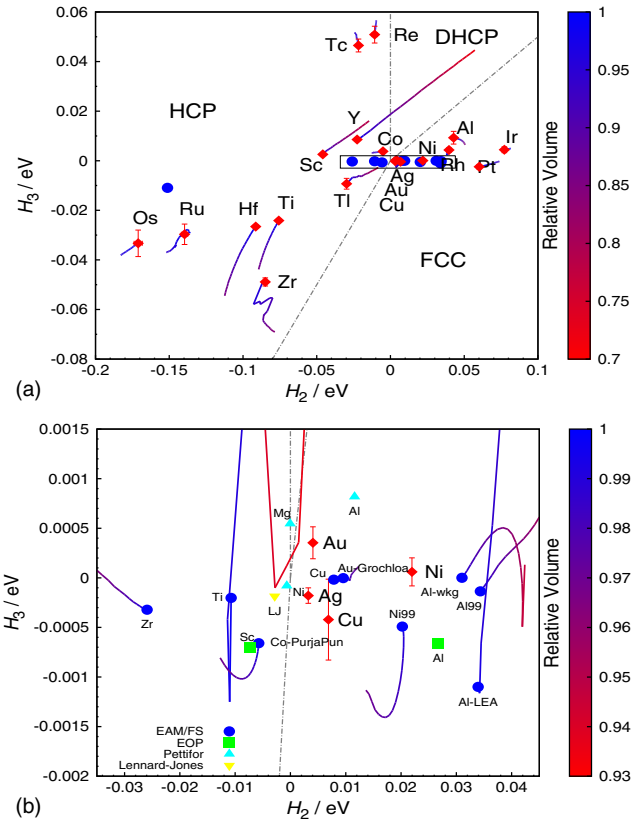

FIG. 2. (a) Figure showing close packed materials plotted against their (H_2, H_3). Lines show the movement under pressure according to DFT calculations. Blue dots show the position of interatomic potentials at equilibrium volume. The outlying interatomic potential is Fortini's Ru EAM potential [8]. The regions of fcc, hcp, and dhcp stability shown assume that H_4 and higher terms are zero. (b) Expanded view of the position of interatomic potentials in the region of H_2-H_3 space bound by the rectangle in (a). The lines again show the effects of compression.

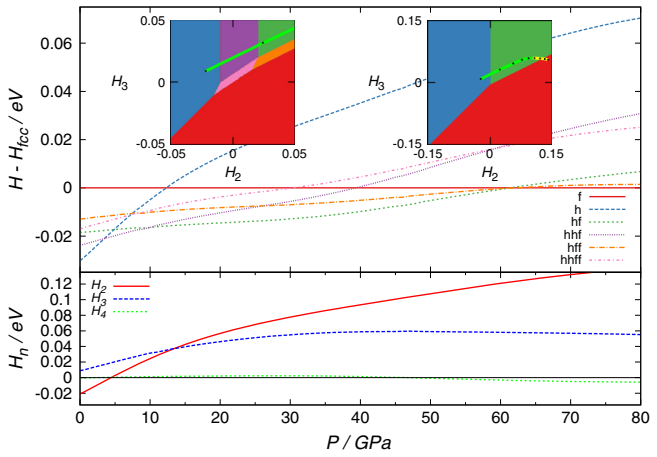

FIG. 3. (top) DFT calculated enthalpies for phases of yttrium with pressure. (bottom) Fitted H_n values with pressure. The insets are colored to show the stable phase for given (H_2, H_3) using the same color scheme; when H_4 is positive (left), all six phases appear, for negative H_4 (right) only fcc, hcp, and dhcp are possible. The line shows changing values of (H_2, H_3) with pressure. Because H_4 for Y is also pressure dependent, this is a projection onto the plane of constant H_4 which it intersects: the line is colored green when the $H_4 > 0$ and yellow when $H_4 < 0$ to show that it passes through the wedge of hhf stability, but not hff. Small dots indicate 10 GPa intervals.

can glide easily and Group 11 materials are soft and malleable.

Yttrium is a particularly interesting case, its pressure trajectory moves it from hcp stability into the dhcp phase (see Fig. 2). Experimentally [10,11], yttrium does this via an intermediate Sm-type phase, also called 9R, which consists of 9 layers: ABACACBCB (Table I). 9R lies on the boundary of the hcp phase with the dhcp phase in Fig. 1 and its stability wedge exists only for $H_4 > 0$. Figure 3 shows that Y has $H_4 > 0$, so the 9R region must be traversed as an intermediate phase between hcp and dhcp, as observed.

Qualitatively, we find that yttrium transforms from hcp to 9R at 4 GPa, then to dhcp at around 10 GPa (Fig. 3). These numbers agree with other DFT calculations [12,13] but are lower than observed experimental pressures, which might be due to hysteresis since the experiments were done with increasing pressure only.

Scandium and thallium appear to behave similarly to yttrium (see Supplemental Material [14]), but Sc is known to transform to a complex non-close-packed structure at a lower pressure than where its trajectory would cross the hcp-dhcp boundary in Fig. 2(a). The trajectory for thallium goes towards the transition line with pressure, but $H_4 < 0$ so it passes below the origin and hcp-fcc is the only observed transition.

The 9R and fcc structures are not adjacent in Fig 1. Therefore, no thermodynamic phase boundary can exist between 9R and fcc. This prohibition of pressure-driven transitions in any system is curious because such transitions have been reported in lithium and sodium. However, Li 9R was very recently proved not to be stable [15], and we find both Li and Na to be more stable in fcc than 9R at all pressures. By contrast, the 9R phase is adjacent to hcp and dhcp, (Fig. 1), so its presence in the samarium phase diagram and in the lanthanide sequence dhcp/9R/hcp/fcc [16,17] are also consistent with the model.

Figure 4 shows that the c/a ratio is strongly correlated with a material's preference for the hcp or fcc phase (H_2). Typically, hcp materials have $c/a < \sqrt{2/3}$, whereas metastable structures of fcc materials have larger than ideal c/a. Curiously, the primary effect of pressure is to move c/a towards ideal, irrespective of the change in H_2 (Sc being an exception).

The H_2 and H_3 values for a selection of interatomic potentials are displayed alongside the first principles data (Fig. 2). We used the Lennard Jones potential, a set of embedded atom and Finnis-Sinclair potentials [8,18–24], the empirical oscillating potential [25], and Pettifor's three

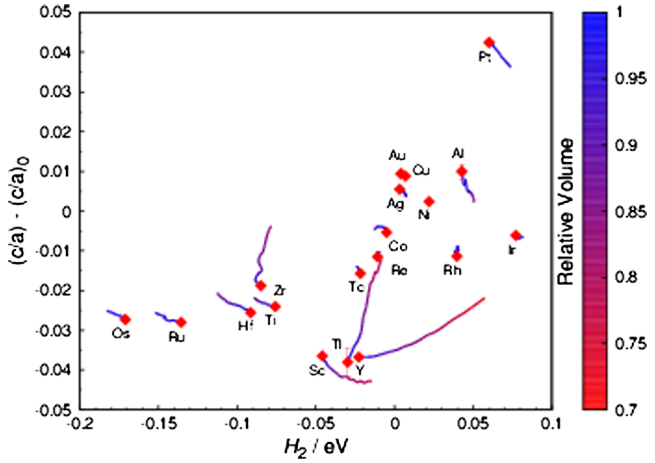

FIG. 4. Correlation between the stability of hcp over fcc (H_2) and the divergence from the ideal close packed ratio of $(c/a)_0 = \sqrt{\frac{2}{3}}$. The effect of pressure up to 20 GPa is again shown as paths colored to correspond to the relative volume.

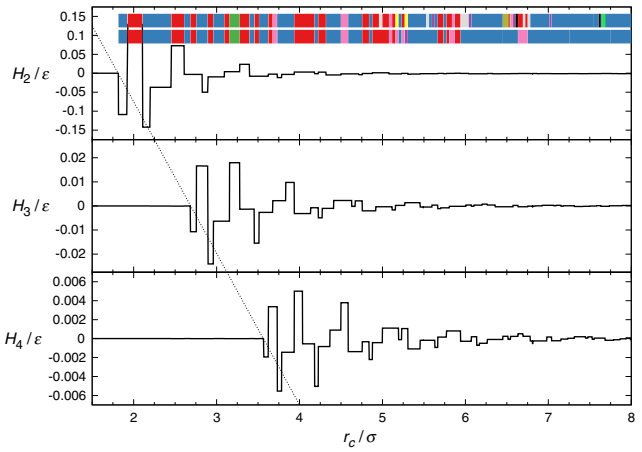

FIG. 5. Zero-pressure H_2, H_3, and H_4 for the Lennard-Jones potential as a function of the interaction range. The diagonal dotted line demonstrates the regular introduction of new H_i series at intervals of the interplanar spacing. The upper of the two ribbons at the top of the graph shows the minimum enthalpy structure at each value of the cutoff, the lower shows the minimum enthalpy structure predicted by Eq. (2) using the H_n values up to $n = 4$. The different colors represent different structures described using the hf notation as follows: red, `f`; blue, `h`; green, `hf`; purple, `hhf`; yellow, `hhhf`; pink, `hhff`; white, `hhfff`; olive, `hhhhhf`; lime, `hhhhff`; cyan, `hhhhhhf`; brown, `hhhhfff`; black, `hhffhhf`.

term oscillating potential for Al, Na, and Mg [26,27] as implemented in the LAMMPS code [28]. Remarkably, these potentials almost all fall into a narrow region of Fig. 2(a), shown expanded in Fig. 2(b), the spread on H_3 being some 2 orders of magnitude smaller than for the DFT calculations.

This weak dependence of enthalpy on stacking sequence implies low basal-plane stacking faults, which leads to systematic erroneously low barriers to basal slip. Furthermore, the phase stability is highly sensitive to pressure and to the details of the empirical potentials.

We find truly remarkable results for the Lennard Jones 6-12 forcefield (Fig 5). This most widely used of potentials is in practice invariably applied with truncation [28], at some range r_{cut}, i.e.,

$$\phi(r) = 4\epsilon\left[\left(\frac{\sigma}{r}\right)^{12} - \left(\frac{\sigma}{r}\right)^{6}\right]H(r_{\mathrm{cut}} - r), \qquad (3)$$

with H the Heaviside function and ϵ and σ defining length and energy units. As $r_{\mathrm{cut}} \to \infty$, H_2 converges to a value of around -0.0009ϵ, which accounts for most of the difference in energy between the fcc and hcp phases. However, the dependence of the H_n values on r_{cut} is erratic; discontinuities occur as new coordination shells come within range, with even H_2 changing sign five times. This means that a large number of minimum enthalpy phases are observed as a function of the cutoff, as indicated in Fig. 5. An alternative truncation with the energy and force shifted to remove the discontinuities at the cutoff distance, is better behaved, but still undergoes five transformations with increasing cutoff, with regions of fcc, hcp, and dhcp phases (see Supplemental Material [14]).

The interatomic potentials exhibit more pressure induced phase transitions than the DFT calculations. We propose that this is because they have a fixed characteristic length scale associated with the zero pressure fitting data. In reality, the characteristic length for metallic interactions is the Fermi wavelength, which reduces with pressure. The long-ranged oscillations of Pettifor potentials scale with the Fermi vector, meaning that the position of shells of neighboring atoms is unchanged relative to the maxima and minima of the potential [27]. Consequently, Pettifor potentials show fewer pressure-induced transitions than other models.

There are similarities with the long-ranged 1D Ising model [9,29,30], in which possible stackings (here h and f) are represented by spins [31–35]. In that case H_2 maps to the field, while the Ising interaction terms are linear combinations of our H_i. The Ising representation turns out to be less useful because it converges slowly. To understand why, consider the strings ABACB and ABABC, which give .hff. and .hhf. for the Ising representation. In the first case the next neighbor hf interaction is between unlike (BC) layers, in the second between like (BB) layers. In the physical system, the set of separations between atoms in B-C is different from B-B, and the associated enthalpy differences are well represented by H_i. In the Ising picture, this difference emerges from correlations between longer range interactions, which have an unintuitive mathematical origin.

In summary, we showed that different stackings of monatomic close packed metals can be uniquely described by a set of structure-specific continuous variables α_n, and that an enthalpy expansion in these quantities leads to a

multidimensional H_n space containing regions of stability for all stackings. The material-specific fitted expansion coefficients H_n converge quickly with n, and allow the stablest structure to be determined. Changes in H_n with pressure allow us to identify phase transformations.

Using the model, we predict that a boundary between fcc and 9R (α−Sm-type) phases cannot exist in any phase diagram, requiring a reassessment of stability of the reported 9R in Na and Li, but not in the Sm prototype. We reproduce and interpret the phase transformation sequence in Y, Sc, and Tl. We identify excess polytypism as problematic for simple interatomic potentials in general, and demonstrate an unprecedented amount of polytypism in the Lennard-Jones system.

Data from the calculation are available from the Edinburgh data store [36].

G. J. A. acknowledges support from a Royal Society Wolfson Award, and the ERC Grant Hecate. C. H. L. thanks EPSRC CM-CDT Grant No. EP/L015110/1. Computing resources provided by EPSRC via UKCP Grant No. EP/P022790/1.

Note added.—Recently, we became aware of a forthcoming paper which also investigates cutoff effects in Lennard-Jonesium [37].

[1] J. Kepleri, *The Six-Cornered Snowflake*, 1966 translation by C. Hardie (Clarendon Press, Oxford, 1611), ISBN: 0198712499.
[2] T. C. Hales and S. P. Ferguson, *The Kepler Conjecture: The Hales-Ferguson Proof* (Springer, New York, 2011), ISBN.
[3] J. Christian and V. Vitek, Rep. Prog. Phys. **33**, 307 (1970).
[4] A. N. Jackson, A. D. Bruce, and G. J. Ackland, Phys. Rev. E **65**, 036710 (2002).
[5] A. Jain, S. P. Ong, G. Hautier, W. Chen, W. D. Richards, S. Dacek, S. Cholia, D. Gunter, D. Skinner, G. Ceder *et al.*, APL Mater. **1**, 011002 (2013).
[6] S. J. Clark, M. D. Segall, C. J. Pickard, P. J. Hasnip, M. I. J. Probert, K. Refson, and M. C. Payne, Zeitschrift für Kristallographie - Crystalline Materials **220**, 567 (2009).
[7] J. P. Perdew, K. Burke, and M. Ernzerhof, Phys. Rev. Lett. **77**, 3865 (1996).
[8] A. Fortini, M. I. Mendelev, S. Buldyrev, and D. Srolovitz, J. Appl. Phys. **104**, 074320 (2008).
[9] M. E. Fisher and W. Selke, Phys. Rev. Lett. **44**, 1502 (1980).
[10] Y. K. Vohra, H. Olijnik, W. Grosshans, and W. B. Holzapfel, Phys. Rev. Lett. **47**, 1065 (1981).
[11] W. A. Grosshans, Y. K. Vohra, and W. B. Holzapfel, J. Magn. Magn. Mater. **29**, 282 (1982).
[12] Y. Chen, Q.-M. Hu, and R. Yang, Phys. Rev. B **84**, 132101 (2011).
[13] Y. Chen, Q.-M. Hu, and R. Yang, Phys. Rev. Lett. **109**, 157004 (2012).
[14] See Supplemental Material at http://link.aps.org/supplemental/10.1103/PhysRevLett.119.205701 for details of DFT calculations for Scandium and Thallium, and the phase behaviour of the shifted and tilted Lennard Jones potential.
[15] G. J. Ackland, M. Dunuwille, M. Martinez-Canales, I. Loa, R. Zhang, S. Sinogeikin, W. Cai, and S. Deemyad, Science **356**, 1254 (2017).
[16] K. Gschneidner and R. Valletta, Acta Metall. **16**, 477 (1968).
[17] W. Holzapfel, J. Alloys Compd. **223**, 170 (1995).
[18] G. Grochola, S. P. Russo, and I. K. Snook, J. Chem. Phys. **123**, 204719 (2005).
[19] G. J. Ackland, Philos. Mag. A **66**, 917 (1992).
[20] J. M. Winey, A. Kubota, and Y. M. Gupta, Model. Simul. Mater. Sci. Eng. **18**, 029801 (2010).
[21] Y. Mishin, D. Farkas, M. J. Mehl, and D. A. Papaconstantopoulos, Phys. Rev. B **59**, 3393 (1999).
[22] X.-Y. Liu, F. Ercolessi, and J. B. Adams, Model. Simul. Mater. Sci. Eng. **12**, 665 (2004).
[23] M. I. Mendelev, M. J. Kramer, C. A. Becker, and M. Asta, Philos. Mag. **88**, 1723 (2008).
[24] G. P. Purja Pun and Y. Mishin, Phys. Rev. B **86**, 134116 (2012).
[25] M. Mihalkovič and C. L. Henley, Phys. Rev. B **85**, 092102 (2012).
[26] D. G. Pettifor and M. A. Ward, Solid State Commun. **49**, 291 (1984).
[27] D. Pettifor, *Bonding and Structure of Molecules and Solids*, Oxford Science Publications (Clarendon, Oxford, 1995).
[28] S. Plimpton, J. Comp. Physiol. **117**, 1 (1995).
[29] P. Bak and J. von Boehm, Phys. Rev. B **21**, 5297 (1980).
[30] J. Yeomans, Solid State Phys. **41**, 151 (1988).
[31] C. Cheng, R. Needs, and V. Heine, J. Phys. C **21**, 1049 (1988).
[32] C. Cheng, R. Needs, V. Heine, and N. Churcher, Europhys. Lett. **3**, 475 (1987).
[33] P. Denteneer and W. Van Haeringen, J. Phys. C **20**, L883 (1987).
[34] M. Plumer, K. Hood, and A. Caillé, J. Phys. C **21**, 4189 (1988).
[35] L. Vitos, P. A. Korzhavyi, and B. Johansson, Phys. Rev. Lett. **96**, 117210 (2006).
[36] DOI: 10.7488/ds/2236.
[37] L. B. Partay, C. Ortner, A. P. Bartok, C. J. Pickard, and G. Csanyi, Phys. Chem. Chem. Phys. **19**, 19369 (2017).